PHYSICAL REVIEW B **87**, 024419 (2013)

Spin-filtering efficiency of ferrimagnetic spinels $CoFe_2O_4$ and $NiFe_2O_4$

Nuala M. Caffrey,[1,*] Daniel Fritsch,[2] Thomas Archer,[1] Stefano Sanvito,[1] and Claude Ederer[3,†]
[1]*School of Physics and CRANN, Trinity College, Dublin 2, Ireland*
[2]*H. H. Wills Physics Laboratory, University of Bristol, Tyndall Avenue, Bristol BS8 1TL, United Kingdom*
[3]*Materials Theory, ETH Zürich, Wolfgang-Pauli-Strasse 27, 8093 Zürich, Switzerland*
(Received 11 January 2013; published 25 January 2013)

We assess the potential of the ferrimagnetic spinel ferrites $CoFe_2O_4$ and $NiFe_2O_4$ to act as spin filtering barriers in magnetic tunnel junctions. Our study is based on the electronic structure calculated by means of first-principles density functional theory within different approximations for the exchange correlation energy. We show that, in agreement with previous calculations, the density of states suggests a lower tunneling barrier for minority spin electrons, and thus a negative spin-filter effect. However, a more detailed analysis based on the complex band structure reveals that both signs for the spin-filtering efficiency are possible, depending on the band alignment between the electrode and the barrier materials and depending on the specific wave-function symmetry of the relevant bands within the electrode.

DOI: 10.1103/PhysRevB.87.024419 PACS number(s): 75.47.−m

I. INTRODUCTION

The ability to generate and detect spin-polarized currents is a central requirement for any practical spintronics device. A promising approach to achieve this goal is to use tunnel junctions containing ferro- or ferrimagnetic barrier materials, thus presenting different tunneling probabilities for majority (spin-up, ↑) and minority (spin-down, ↓) electrons. Efficient spin-filtering has been demonstrated for ferromagnetic insulators such as EuS,[1] EuO,[2] and $BiMnO_3$.[3] However, the magnetic ordering temperatures of these magnets are rather low. Therefore the identification of suitable barrier materials that operate at room temperature or above is of great interest.

Spinel ferrites are insulating ferrimagnets with high Curie temperatures ($T_C = 790$ K for $CoFe_2O_4$ and 865 K for $NiFe_2O_4$),[4] and therefore are promising candidates for efficient room-temperature spin filtering. A measure of the ability of a material or a device to select a particular spin direction is the spin-filtering efficiency P_{sf}, which is defined as

$$P_{sf} = \frac{I^{\uparrow} - I^{\downarrow}}{I^{\uparrow} + I^{\downarrow}},$$

where I^{σ} is the spin-σ component of the current, which is assumed to be carried by the two spin species in parallel. Recent experiments on ferrimagnetic spinels appear promising, as a spin-filtering efficiency of +22% has been measured for $NiFe_2O_4$ at low temperatures.[5] The measured positive sign of P_{sf} is in apparent contradiction with results of band-structure calculations, demonstrating that the bottom of the conduction band is lower for spin-down electrons than for spin-up,[6] which would lead to a lower tunneling barrier for minority-spin electrons. It was suggested that this apparent discrepancy could be due to effects related to the wave-function symmetry of the tunneling states.[5] Furthermore, for $CoFe_2O_4$, both positive and negative P_{sf} have been reported in junctions made of different electrode materials and where P_{sf} was measured with different experimental techniques. The reported values of P_{sf} range from −44% to +26%.[7–12] Due to these large variations in experimental results (with both signs occurring for the spin-filtering efficiency), a conclusive picture of spin-filtering in spinel ferrites has not emerged, yet. As such, a first-principles investigation of the spin-filtering efficiency in these materials is highly desirable, in order to provide a reference for future experimental studies and to allow further optimization of the corresponding devices.

So far, theoretical predictions for the spin-filter effect in $CoFe_2O_4$ and $NiFe_2O_4$ are almost exclusively based on density of states (DOS) calculations within a self-interaction corrected (SIC) local spin-density approximation (LSDA).[6] The spin-splitting of the conduction band minimum (CBM) in these calculations suggests a lower tunnel barrier for minority-spin electrons and thus a negative sign for the spin-filtering efficiency. However, it is well known that in many cases, this simple density of states argument can be misleading, and the tunnel probability can be strongly dependent on the specific wave-function symmetry.[13] The implications of this were first noticed in a Fe/MgO/Fe heterostructure,[14,15] where symmetry-dependent tunneling results in half-metallic behavior of the Fe/MgO(001) stack. Since then, the so-called *complex band structure*, which determines the decay length of Bloch states with different wave-function symmetries inside an insulating barrier, has been used to account for many, otherwise unexplained, experimental results in spin-dependent tunnel junctions. Furthermore, it is of interest to compare the SIC-LSDA result of Ref. 6 to the electronic structure obtained by using alternative approaches such as LSDA + U, hybrid functionals, or other SIC approaches.

Here, we present a detailed comparison of the electronic structure of $CoFe_2O_4$ and $NiFe_2O_4$ calculated within different approximations for the exchange-correlation potential. This allows us to identify features of the DOS that are fairly robust with respect to the specific choice of exchange-correlation potential and features that are very sensitive to this choice. In addition, we calculate the complex band-structure for both materials within the atomic SIC method (ASIC),[16,17] which facilitates the identification of suitable electrode materials that can lead to high spin-filtering efficiency. We show that, for both $CoFe_2O_4$ and $NiFe_2O_4$ and the two transport directions [001] and [111], electrons tunnel with the highest probability at the center of the two-dimensional Brillouin zone in the plane orthogonal to the transport direction. Furthermore, depending on

the exact alignment of the electrode Fermi level relative to the CBM of the barrier, the tunneling current may present either a predominant majority or a predominant minority contribution, i.e., P_{sf} may change sign depending on the level alignment.

The paper is organized as follows. After having briefly presented the computational method and the details of the crystallographic unit cell used for this study, we proceed to describe the electronic structure of $CoFe_2O_4$ and $NiFe_2O_4$. In particular, we first discuss the DOS and real band structures, and then move on to present the complex ones. The final section summarizes our main conclusions.

II. METHODS

We employ the VASP[18] and SIESTA[19] density functional theory (DFT) code packages for the calculation of DOS and real band structures and the SMEAGOL code[20,21] to calculate the complex band structure. The VASP calculations have been performed by using the projector-augmented wave (PAW) method[22] with standard PAW potentials supplied with the VASP distribution, a 500 eV plane wave energy cutoff, and a Γ centered $6 \times 6 \times 6$ k-point mesh for the Brillouin zone sampling. We employ the generalized gradient approximation (GGA) according to the Perdew-Burke-Ernzerhof formulation[23] together with the Hubbard "$+U$" correction,[24] where $U = 3$ eV and $J = 0$ eV is applied to the d states of all transition metal cations, as well as the hybrid functional approach according to Heyd, Scuseria, and Ernzerhof (HSE),[25] using the standard choice for the fraction of Hartree-Fock exchange ($\alpha = 0.25$) and a reduced plane-wave energy cutoff of 400 eV. When using the localized basis set code SIESTA, structural relaxations were performed using the GGA while the atomic self-interaction correction (ASIC) scheme was used to determine the electronic structure, including the complex band structure. A $6\times6\times6$ k-point Monkhorst-Pack mesh was used to converge the density matrix to a tolerance of 10^{-5} and a grid spacing equivalent to a plane-wave cutoff of 800 eV was used.

For most of our calculations, we use the smallest possible unit cell (containing 2 formula units) to describe the inverse spinel structure. The corresponding distribution of cations on the spinel B site lowers the space group symmetry from $Fd\bar{3}m$ to $Imma$.[26] We also present some results obtained for a cation distribution with $P4_122$ symmetry, which requires a doubling of the unit cell to 4 formula units (the k-point sampling is then adjusted accordingly). We have previously shown that both $Imma$ and $P4_122$ are low-energy configurations for the inverse spinel structure in $CoFe_2O_4$ and $NiFe_2O_4$ and that the specific cation arrangement has only a minor influence on the global electronic structure of these systems.[27] We note that experimentally a disordered distribution of Fe^{3+} and Co^{2+}/Ni^{2+} cations over the spinel B site with effective cubic $Fd\bar{3}m$ symmetry, i.e., with no long-range cation order, is generally observed, even though recently indications for short range cation order in both $NiFe_2O_4$ bulk and thin film samples have been reported.[28,29] For a more detailed comparison between the different cation configurations see Refs. 27 and 30.

Structural relaxations have been performed at the GGA level, with all cations being fixed to their ideal cubic positions.[26] The relaxed bulk lattice constants a_0 obtained

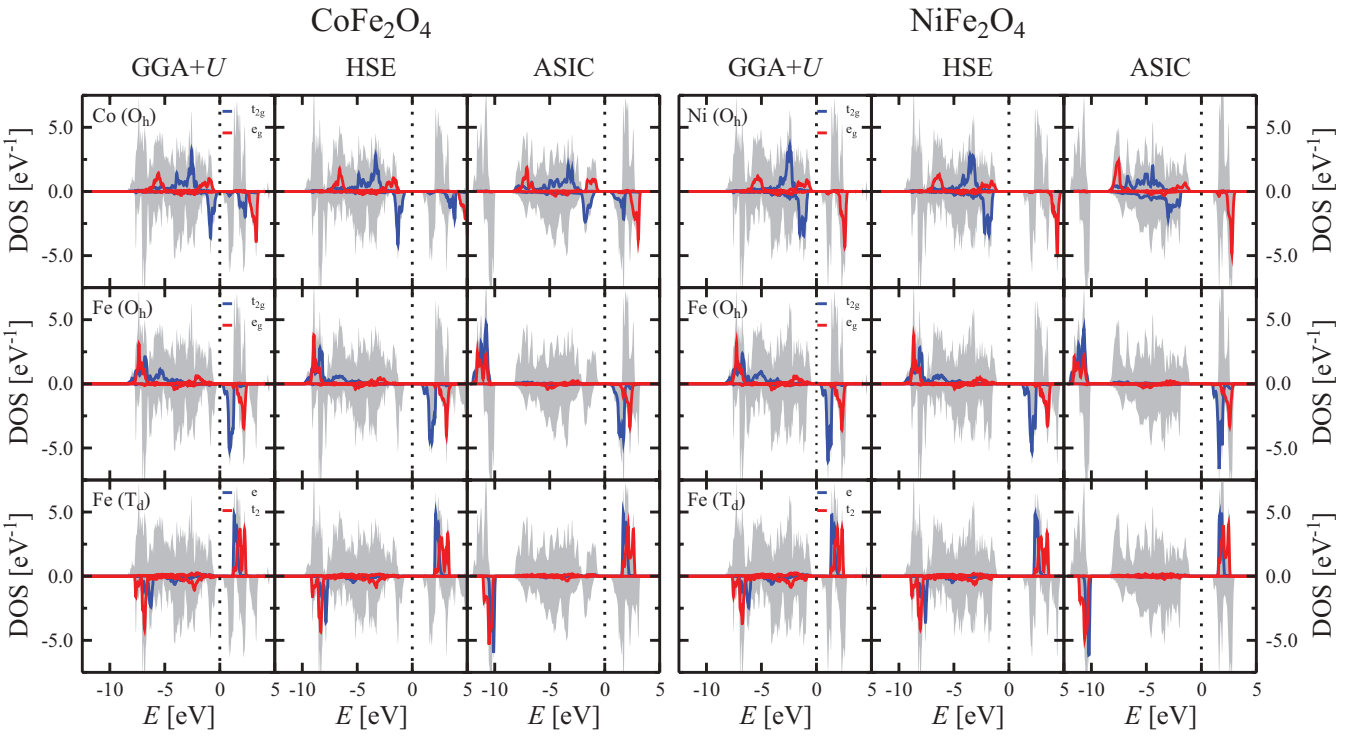

FIG. 1. (Color online) Total and projected DOS per formula unit for $CoFe_2O_4$ (left) and $NiFe_2O_4$ (right) calculated with different exchange-correlation potentials (from left to right: GGA + U, HSE, and ASIC). The t_{2g} and e_g states of Fe, Co, and Ni on the O_h sites and the e and t_2 states of Fe on the T_d sites are shown as black (blue) and dark grey (red) lines, respectively. The shaded grey area in all panels depicts the total DOS. Minority spin projections are shown using negative values. The zero energy is set to the middle of the band gap.

TABLE I. Band gap (E_g) and spin splitting of the CBM (ΔCBM) for $CoFe_2O_4$ and $NiFe_2O_4$ calculated with different exchange-correlation functionals. All values are in electron volts.

	$CoFe_2O_4$		$NiFe_2O_4$	
	E_g	ΔCBM	E_g	ΔCBM
GGA + U	0.52	0.92	0.83	0.86
HSE	1.60	1.09	2.32	1.00
ASIC	1.08	1.00	2.07	0.46

by using VASP (SIESTA) are 8.366 Å (8.360 Å) and 8.346 Å (8.356 Å) for $CoFe_2O_4$ and $NiFe_2O_4$, respectively, and are in very good agreement with experimental data (see Ref. 27, and references therein).

III. RESULTS AND DISCUSSION

A. Electronic structure

It has been previously shown that GGA leads to a half-metallic solution for $CoFe_2O_4$ and results in only a very small insulating gap in the case of $NiFe_2O_4$ (see, e.g., Refs. 26 and 31 and references therein). The DOS of $CoFe_2O_4$ and $NiFe_2O_4$ calculated by using a selection of beyond-GGA functionals are depicted in Fig. 1. It can be seen that all the studied exchange-correlation potentials lead to an insulating state for $CoFe_2O_4$ and an enhanced band gap for $NiFe_2O_4$. When compared to the GGA + U band gaps, both the inclusion of Hartree-Fock exchange within the HSE calculation as well as the ASIC treatment lead to a large increase in the band gap values for both the Co and Ni based ferrite, with the largest band gaps obtained for HSE (see Table I). We also note that our results are consistent with recent HSE and LSDA + U calculations for $NiFe_2O_4$.[32]

Going into more details we notice that, while the occupied DOS is very similar for GGA + U and HSE, the ASIC method places the local Fe spin-majority states significantly lower in energy. This results in a gap between these Fe states and the higher-lying Co (Ni) d and oxygen p valence bands. Interestingly, for $CoFe_2O_4$, the valence band maximum in ASIC is made up of the majority spin Co e_g states, whereas for both GGA + U and HSE, the corresponding minority spin t_{2g} states are slightly higher in energy. We also note that the difference in the calculated GGA + U band gap of $CoFe_2O_4$ ($NiFe_2O_4$) compared to the previously obtained values of 0.9 eV (0.97 eV) for the $Imma$ structure,[26] and 1.24 eV (1.26 eV) for the $P4_122$ structure,[27] is due to the fact that in the present work, all calculations are performed at the GGA volume, whereas the calculations in Refs. 26 and 27 have been performed at the larger GGA + U optimized volume. In addition to the expected dependence of the calculated band gaps on the exchange correlation potential, our results thus also indicate a strong volume sensitivity of the gap, in particular for $CoFe_2O_4$. Experimental estimates for the band gaps of spinel ferrites are sparse and vary over a broad range comprised between 0.11 and 1.5 eV for $CoFe_2O_4$ and between 0.3 and 3.7 eV for $NiFe_2O_4$.[33,34] A recent optical absorption study of $NiFe_2O_4$ suggests an indirect gap of 1.6 eV in the minority-spin channel,[32] which thus represents an upper bound for the corresponding fundamental band gap.

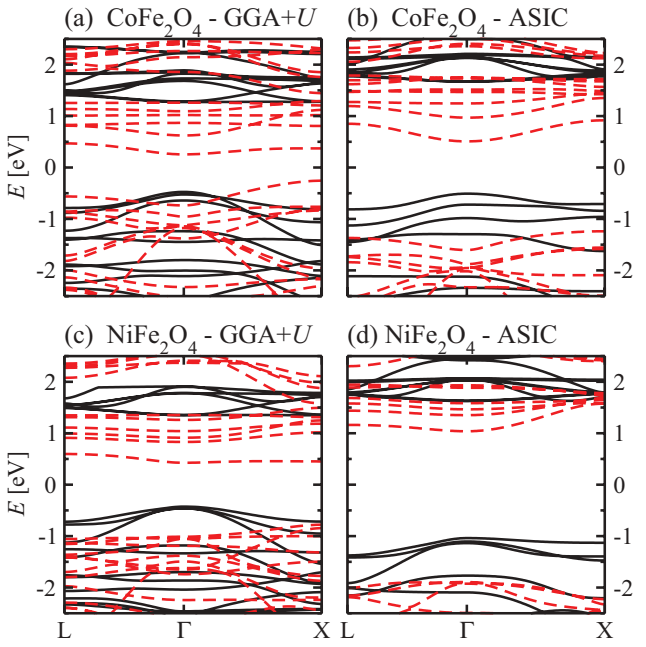

FIG. 2. (Color online) Band structures for energies around the band gap of $CoFe_2O_4$ [top (a) and (b)] and $NiFe_2O_4$ [bottom (c) and (d)] calculated by using the GGA+U exchange-correlation functional [left (a) and (c)] and the ASIC scheme [right (b) and (d)]. Majority- and minority-spin bands are shown as full (black) and dashed (red) lines.

In all cases and for both $CoFe_2O_4$ and $NiFe_2O_4$, the CBM is lower in energy for the spin-down states than for spin-up ones, in agreement with the SIC-LSDA calculations of Ref. 6. In the case of $CoFe_2O_4$, all the three approaches used in our work predict a spin splitting of the CBM (ΔCBM in Table I) of around 1 eV. For $NiFe_2O_4$, however, GGA + U and HSE yield a ΔCBM of around 0.9–1.0 eV, while ASIC gives a somewhat smaller splitting of only 0.46 eV. In all the cases, the obtained spin splittings of the CBM are smaller than those reported in Ref. 6, 1.28 eV (1.21 eV) for $CoFe_2O_4$ ($NiFe_2O_4$). We note, however, that even smaller values, namely 0.47 eV for both $CoFe_2O_4$ and $NiFe_2O_4$, have been obtained in previous GGA + U calculations at the relaxed GGA + U volume.[27] Recent experiments estimate the spin splitting of the CBM in the tens of meV range for $CoFe_2O_4$-containing junctions.[9]

In order to shed further light on the nature of the bands around the gap, the calculated GGA + U and ASIC band structures for both $CoFe_2O_4$ and $NiFe_2O_4$ are shown in Fig. 2. Apart from the larger band gaps obtained by the ASIC approach, it can be seen that the relative energies of the minority and majority spin bands in the upper valence band region for $CoFe_2O_4$ differ between GGA + U and ASIC. This is consistent with our previous discussion of the DOS. For the calculation that is performed with GGA + U, the top of the valence band is formed by a minority spin band with maximum at the X point, i.e., the minority spin band gap is indirect. In contrast a direct gap with mixed spin character at Γ is obtained by ASIC. Since, as we will show in the following, the tunneling probabilities are dominated by states

around the Γ point, we do not expect that this qualitative difference between the two exchange-correlation functionals will critically affect the transport properties.

Based on our analysis of the DOS and the band structure in the vicinity of the gap, we can conclude that despite some differences, all computational methods consistently predict a lower tunnel barrier for the minority spin electrons and therefore a negative spin-filtering efficiency for both $CoFe_2O_4$ and $NiFe_2O_4$. However, as shown in Fe/MgO/Fe tunnel junctions,[14,15] in the case of high-quality epitaxial interfaces between the electrodes and the barrier material, such DOS considerations are only of limited value for the description of actual transport properties. Instead, the specific symmetry of the decaying wave functions inside the barrier has to be considered. This can be achieved through calculation of the complex band structure.[13]

B. Complex band structure

The complex band structure along a particular crystalline direction is calculated with the DFT nonequilibrium Green's function code SMEAGOL.[20,21] The complex band structure is nothing but the solution of the secular band equation extended to imaginary wave vectors. Let us assume that the transport direction of a given tunnel junction is along the z direction and that the material composing the barrier has a particular crystalline axis aligned along that direction. For any given k vector in the transverse x-y plane, $k_\parallel = (k_x,k_y)$, and for any energy, E, the band equation $E = E(k_x,k_y,k_z)$ can be solved for k_z if one admits imaginary solutions $k_z = q + i\kappa$. This means that the wave function of an electron approaching the tunneling barrier with transverse wave vector $k_\parallel$ exponentially decays into the barrier along the z direction over a length-scale given by $1/\kappa$. Clearly, such decay rate depends on the transverse k vector and the energy, i.e., $\kappa = \kappa(k_x,k_y;E)$. Here, we consider the situation of electron transport along both the [001] and [111] directions of the cubic spinel structure.

In Fig. 3, we plot the minimal value of κ as a function of k_x and k_y (calculated on a 100×100 grid) at different energies within the gap. We include data for both $CoFe_2O_4$ and $NiFe_2O_4$ considering both transport directions for the *Imma* configuration, and we also present data for the $P4_122$ configuration and transport along the [001] direction. The crucial result emerging from Fig. 3 is that in all cases κ is smallest at the Γ point of the two-dimensional Brillouin zone corresponding to the x-y plane. This means that, due to the exponential dependence of the wave function on κ, electron tunneling away from the Γ point will contribute very little to the transport. As such, in the analysis that will follow, we will only consider transport through the Γ point. We note that Γ-point filtering is a highly desirable property for both tunnel junctions and spin injection. As has been shown for the Fe/MgO barrier, as the thickness of the MgO layer increases, so does the selectivity of the Γ point. This in turn increases the tunneling magnetoresistance (TMR). Although the Γ-point filtering is not strictly necessary for a large TMR, it significantly reduces the importance of the material choice for the electrodes.

Having established that the transport predominantly occurs at the Γ point, further insight can be gained by exploring the energy dependence of $\kappa(0,0;E)$. In particular, it is important to establish the spin and orbital symmetry of the complex

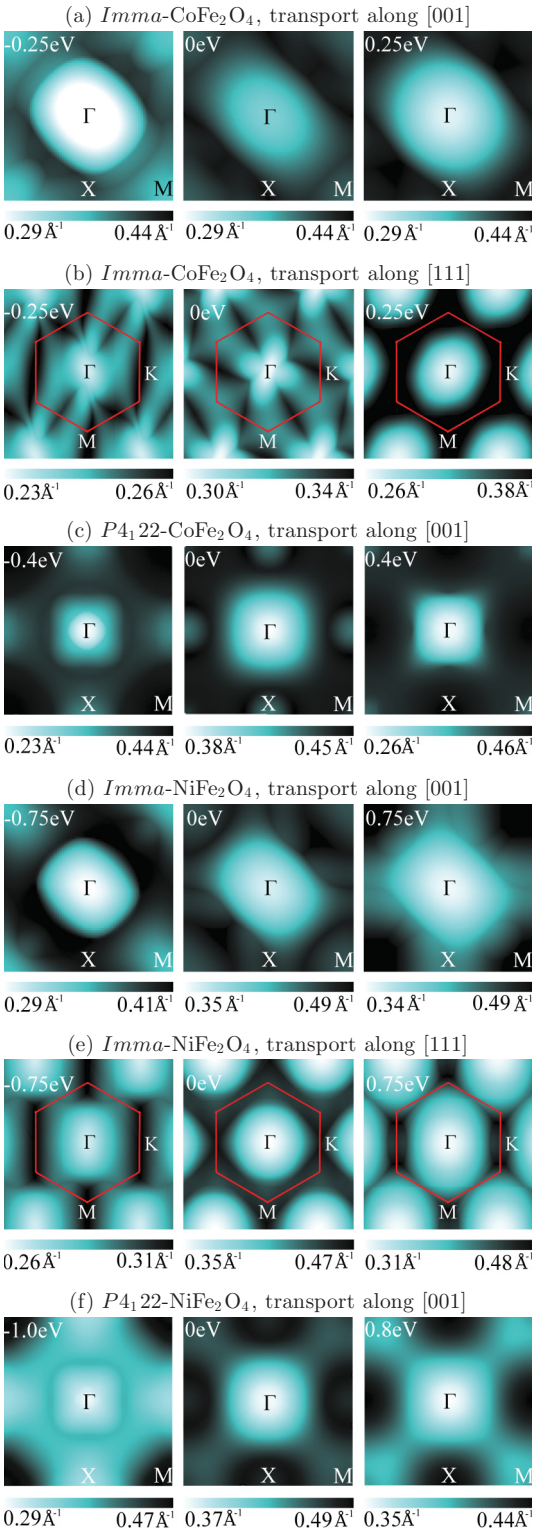

FIG. 3. (Color online) Minimal value of κ at different energies (indicated at the top left in each graph) within the gap for $CoFe_2O_4$ (a)–(c) and $NiFe_2O_4$ (d)–(f) along different transport directions, calculated within the ASIC approach. Zero energy corresponds to the middle of the band gap.

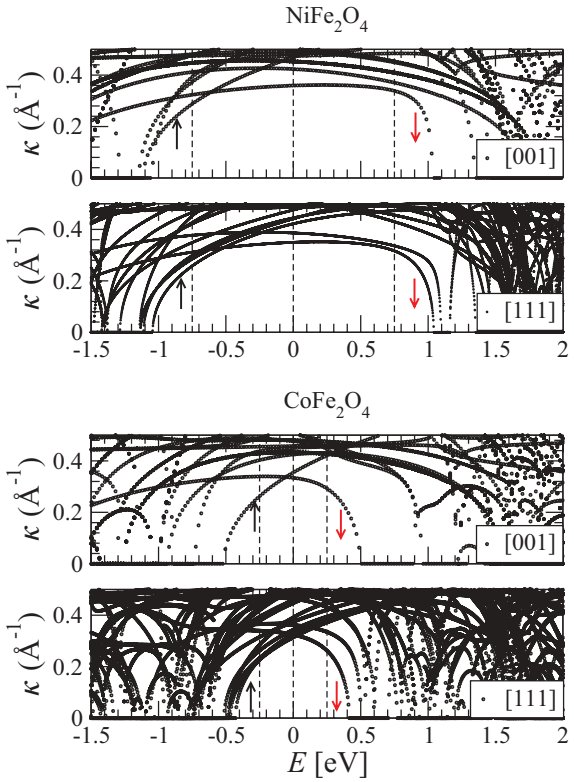

FIG. 4. (Color online) The complex band structure corresponding to $k_x = k_y = 0$ for $NiFe_2O_4$ (upper two panels) and $CoFe_2O_4$ (lower two panels) along [001] and [111], calculated within ASIC for the *Imma* ionic configuration. The up and down arrows indicate the spin character of the lowest lying complex bands. The vertical dashed lines indicate the energies that were used for the k_x-k_y plots in Fig. 3.

bands corresponding to the smallest value of $\kappa(0,0;E)$ for each energy, since incident waves with that particular symmetry will dominate the tunneling current. In Fig. 4, we present the complex band-structures of $CoFe_2O_4$ and $NiFe_2O_4$, calculated along the [001] and [111] directions at the Γ point in the transverse 2D Brillouin zone for the *Imma* configuration. One can easily recognize that for both $CoFe_2O_4$ and $NiFe_2O_4$, the main features, which we discuss in the following, are similar for the two different transport directions. We note that the transport calculation along [111] requires a larger unit cell, in order to obtain lattice vectors that are either perpendicular or parallel to the transport direction, which leads to a larger number of complex bands compared to the [001] case. In both materials, the slowest decay rate close to the valence band maximum corresponds to electrons with majority-spin character (in agreement with the real band structure shown in Fig. 2). This remains the case for energies up to around 0.5 eV from the top of the valence band, although the decay rate increases quickly with energy. In contrast, the lowest decay rate for energies taken in the upper part of the band gap is dominated by states with minority spin symmetry. For $NiFe_2O_4$, this decay rate remains almost constant for a wide energy window of about 1.5 eV, whereas for $CoFe_2O_4$, the gap region is divided more symmetrically between the majority- and minority-spin-dominated regions. The smaller ASIC calculated band gap of $CoFe_2O_4$ compared to that of $NiFe_2O_4$ results in slightly

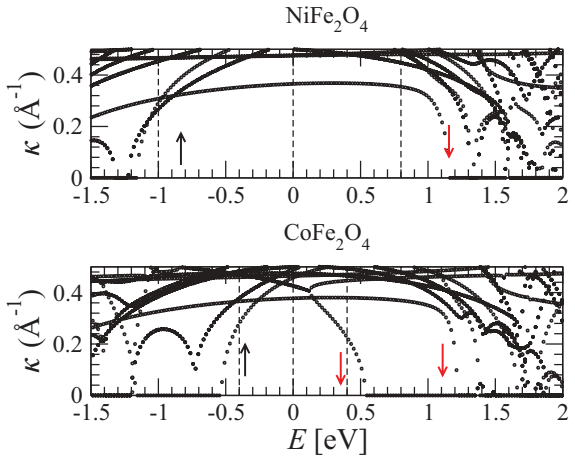

FIG. 5. (Color online) The complex band structure corresponding to $k_x = k_y = 0$ for $NiFe_2O_4$ (upper panel) and $CoFe_2O_4$ (lower panel) along [001] for the $P4_122$ configuration, calculated within ASIC. The up and down arrows indicate the spin-character for some of the lowest lying complex bands.

slower decays within the gap region for both majority and minority spins.

In Fig. 5, we also present the complex band structure of $CoFe_2O_4$ and $NiFe_2O_4$ in the $P4_122$ configuration for transport along [001]. One can recognize the slightly larger band-gap compared to the *Imma* configuration, but for $NiFe_2O_4$, the complex bands look very similar compared to the *Imma* case. For $CoFe_2O_4$, one can see that the bands in the mid-gap region connect in a somewhat different way than in the *Imma* configuration. However, the spin characters of the lowest complex band in the upper and lower gap regions remain unaffected by the different cation distribution, even though the energy range dominated by the minority spin complex bands is somewhat more extended in the $P4_122$ case.

From the complex bands, it becomes clear that positive as well as negative values for P_{sf} are possible for both $NiFe_2O_4$ and $CoFe_2O_4$, depending on whether the Fermi level of the electrode lies in the upper or lower gap region of the spinel tunnel barrier and on the availability of majority or minority spin carriers in the metal. If the Fermi level of the metallic electrode lies within ∼0.5 eV from the top of the valence band, the slowest decay rate in both $CoFe_2O_4$ and $NiFe_2O_4$ will be for electrons with majority spin. In contrast, if the Fermi level of the electrode is more than 0.5 eV above the valence band edge of the spinel barrier, then the slowest decaying state is in the minority spin channel. The exact position of the Fermi level of the metal depends on the band alignment between the two materials. Thus the spin filter efficiency of the spinel ferrite barrier will depend strongly on the band alignment and eventually also on the orbital symmetry of the electrode states at the Fermi level. In addition, a good lattice match is of course required, otherwise translational symmetry is broken in the transverse plane and the complex band-structure argument breaks down. Here, the possibility to grow good quality films of $CoFe_2O_4$ and $NiFe_2O_4$ with either [001] or [111] orientation (see e.g. Refs. 35–37) opens up a wide range of possible electrode materials. In fact, high-quality epitaxial junctions of $CoFe_2O_4$ or $NiFe_2O_4$ with various electrode materials, such

as $La_{2/3}Sr_{1/3}MnO_3$, Au, Fe_3O_4, Nb-doped $SrTiO_3$, Pt, Co, Al, and $SrRuO_3$, have already been fabricated.[5,7–12]

So far, we have only discussed the spin character of the complex bands, whereas it is well known from the Fe/MgO/Fe system that the orbital character of the relevant bands can also have a crucial influence on the tunneling properties. The determination of orbital character of the complex bands in the inverse spinel ferrites $CoFe_2O_4$ and $NiFe_2O_4$ is complicated by the different symmetries of the specific cation configurations used in the calculations. For example, the lowest lying state above the gap at Γ in *Imma*-$NiFe_2O_4$, i.e., the one which connects to the complex band with minority spin character that has the smallest extinction coefficient over a rather large energy region within the gap, transforms according to the fully symmetric irreducible representation A_g of the corresponding orthorhombic point group *mmm*. This means that, assuming an electrode with cubic bulk symmetry, this state can in principle couple to Δ_1 and Δ_2/Δ_2' bands for transport along the [001] direction (whether Δ_2 or Δ_2' depends on how exactly the electrode is oriented with respect to the spinel structure), or to Λ_1 and Λ_3 for transport along the [111] direction. However, these consideration hold only for the case with *Imma* symmetry and it is unclear how different cation arrangements, in particular, a completely disordered cation distribution, would change these symmetry-based selection rules. Generally, the lower symmetry of the various cation arrangements leads to fewer symmetry restrictions regarding the possible coupling with electrode bands. Since a full symmetry analysis of all combinations that can possibly occur is beyond the scope of this paper, we restrict our analysis to the spin character of the decaying states within the barrier, which was discussed in the preceding paragraphs.

IV. SUMMARY AND CONCLUSIONS

In summary, we have calculated the electronic structure of both $NiFe_2O_4$ and $CoFe_2O_4$ using different approaches to evaluate the exchange-correlation potential. These include GGA, GGA + U, HSE, and ASIC. We found that while there are certain characteristic differences in the predicted band structure, the densities of states of all beyond-GGA methods consistently suggest a lower tunnel barrier for minority-spin electrons. Due to the well-known limitations of this simple density of states picture of tunneling, we have further analyzed the complex bands of the two materials at the ASIC level.

We have shown that the tunneling along the [001] and [111] directions is dominated by zone-center contributions ($k_x = k_y = 0$), and that for both $NiFe_2O_4$ and $CoFe_2O_4$, the spin character of the slowest decaying state changes within the gap. Therefore $NiFe_2O_4$ and $CoFe_2O_4$ are both capable of acting as either positive or negative spin filters, depending on the band alignment and wave-function symmetry of the electrodes. Given such a relatively sensitive dependence of the tunneling current on the position of the electrode Fermi level, we envision that gating may allow the spin filtering to be switched from positive to negative.

However, we also want to note that based on the complex band-structure of the barrier alone, it is not possible to make a definite prediction about the transport properties observed in a specific experiment. One may still encounter a situation where incident wave functions with the desired symmetry, i.e., matching that of the smallest $\kappa(0,0;E)$ inside the barrier, are not available within the electrodes, simply because of the corresponding real band structure.[38,39] Furthermore, it has been demonstrated recently for the case of an Fe-$MgAl_2O_4$-Fe tunnel junction, i.e., containing a nonmagnetic spinel as barrier material, that the different unit cell sizes of the spinel barrier and the Fe electrodes can open up new transport channels due to "backfolding" of bands from the in-plane Brillouin zone boundary onto the Γ point.[40] This leads to a relatively low tunnel magnetoresistance for the Fe-$MgAl_2O_4$-Fe junction, even though the corresponding complex and real band structures would indicate a highly symmetry-selective barrier.[40,41] Therefore, in order to fully assess the spin-filter efficiency for a specific combination of electrode and barrier materials, a full transport calculation for the entire device needs to be performed. Nevertheless, the analysis of the complex band-structure provides a powerful interpretative tool and offers a good indication on what are the dominant contributions to the tunneling current. In the present case, it allows the rationalization of both signs of the spin-filter efficiency occurring in $NiFe_2O_4$ and $CoFe_2O_4$ tunnel junction, depending on the band alignment with the electrode.

ACKNOWLEDGMENTS

This work has been supported by Science Foundation Ireland under (Grants SFI-07/YI2/I1051 and 07/IN.1/I945) and by the EU-FP7 (iFOX project). We made use of computational facilities provided by the Trinity Centre for High Performance Computing (TCHPC) and the Irish Centre for High-End Computing (ICHEC).

*Current address: Institute of Theoretical Physics and Astrophysics, Christian-Albrechts-Universität zu Kiel, Leibnizstrasse 15, 24098 Kiel, Germany; caffreyn@tcd.ie

†claude.ederer@mat.ethz.ch

[1] J. S. Moodera, X. Hao, G. A. Gibson, and R. Meservey, Phys. Rev. Lett. **61**, 637 (1988).

[2] T. S. Santos and J. S. Moodera, Phys. Rev. B **69**, 241203 (2004).

[3] M. Gajek, M. Bibes, A. Barthélémy, K. Bouzehouane, S. Fusil, M. Varela, J. Fontcuberta, and A. Fert, Phys. Rev. B **72**, 020406 (2005).

[4] V. A. M. Brabers, in *Handbook of Magnetic Materials*, edited by K. H. J. Buschow (Elsevier, Amsterdam, 1995), pp. 189–324.

[5] U. Lüders, M. Bibes, K. Bouzehouane, E. Jacquet, J.-P. Contour, S. Fusil, J.-F. Bobo, J. Fontcuberta, A. Barthélémy, and A. Fert, Appl. Phys. Lett. **88**, 082505 (2006).

[6] Z. Szotek, W. M. Temmerman, D. Ködderitzsch, A. Svane, L. Petit, and H. Winter, Phys. Rev. B **74**, 174431 (2006).

[7] M. G. Chapline and S. X. Wang, Phys. Rev. B **74**, 014418 (2006).

[8] Y. F. Chen and M. Ziese, Phys. Rev. B **76**, 014426 (2007).

[9] A. V. Ramos, M.-J. Guittet, J.-B. Moussy, R. Mattana, C. Deranlot, F. Petroff, and C. Gatel, Appl. Phys. Lett. **91**, 122107 (2007).
[10] A. V. Ramos, T. S. Santos, G. X. Miao, M. J. Guittet, J. B. Moussy, and J. S. Moodera, Phys. Rev. B **78**, 180402 (2008).
[11] F. Rigato, S. Piano, M. Foerster, F. Giubileo, A. M. Cucolo, and J. Fontcuberta, Phys. Rev. B **81**, 174415 (2010).
[12] Y. K. Takahashi, S. Kasai, T. Furubayashi, S. Mitani, K. Inomata, and K. Hono, Appl. Phys. Lett. **96**, 072512 (2010).
[13] P. Mavropoulos, N. Papanikolaou, and P. H. Dederichs, Phys. Rev. Lett. **85**, 1088 (2000).
[14] W. H. Butler, X.-G. Zhang, T. C. Schulthess, and J. M. MacLaren, Phys. Rev. B **63**, 054416 (2001).
[15] J. Mathon and A. Umerski, Phys. Rev. B **63**, 220403 (2001).
[16] C. D. Pemmaraju, T. Archer, D. Sánchez-Portal, and S. Sanvito, Phys. Rev. B **75**, 045101 (2007).
[17] A. Filippetti, C. D. Pemmaraju, S. Sanvito, P. Delugas, D. Puggioni, and V. Fiorentini, Phys. Rev. B **84**, 195127 (2011).
[18] G. Kresse and J. Furthmüller, Comput. Mat. Sci. **6**, 15 (1996).
[19] J. M. Soler, E. Artacho, J. D. Gale, A. García, J. Junquera, P. Ordejón, and D. Sánchez-Portal, J. Phys.: Condens. Matter **14**, 2745 (2002).
[20] A. R. Rocha, V. M. Garcia-Suarez, S. Bailey, C. Lambert, J. Ferrer, and S. Sanvito, Phys. Rev. B **73**, 085414 (2006).
[21] I. Rungger and S. Sanvito, Phys. Rev. B **78**, 035407 (2008).
[22] P. E. Blöchl, Phys. Rev. B **50**, 17953 (1994).
[23] J. P. Perdew, K. Burke, and M. Ernzerhof, Phys. Rev. Lett. **77**, 3865 (1996).
[24] V. I. Anisimov, F. Aryasetiawan, and A. I. Liechtenstein, J. Phys.: Condens. Matter **9**, 767 (1997).
[25] J. Heyd, G. E. Scuseria, and M. Ernzerhof, J. Chem. Phys. **118**, 8207 (2003).
[26] D. Fritsch and C. Ederer, Phys. Rev. B **82**, 104117 (2010).
[27] D. Fritsch and C. Ederer, Appl. Phys. Lett. **99**, 081916 (2011).
[28] V. G. Ivanov, M. V. Abrashev, M. N. Iliev, M. M. Gospodinov, J. Meen, and M. I. Aroyo, Phys. Rev. B **82**, 024104 (2010).
[29] M. N. Iliev, D. Mazumdar, J. X. Ma, A. Gupta, F. Rigato, and J. Fontcuberta, Phys. Rev. B **83**, 014108 (2011).
[30] D. Fritsch and C. Ederer, Phys. Rev. B **86**, 014406 (2012).
[31] D. Fritsch and C. Ederer, J. Phys.: Conf. Ser. **292**, 012104 (2011).
[32] Q.-C. Sun, H. Sims, D. Mazumdar, J. X. Ma, B. S. Holinsworth, K. R. O'Neal, G. Kim, W. H. Butler, A. Gupta, and J. L. Musfeldt, Phys. Rev. B **86**, 205106 (2012).
[33] R. D. Waldron, Phys. Rev. **99**, 1727 (1955).
[34] R. C. Rai, S. Wilser, M. Guminiak, B. Cai, and M. L. Nakarmi, Appl. Phys. A **106**, 207 (2011).
[35] C. N. Chinnasamy, S. D. Yoon, A. Yang, A. Baraskar, C. Vittoria, and V. G. Harris, J. Appl. Phys. **101**, 09M517 (2007).
[36] A. V. Ramos, J.-B. Moussy, M.-J. Guittet, M. Gautier-Soyer, C. Gatel, P. Bayle-Guillemaud, B. Warot-Fonrose, and E. Snoeck, Phys. Rev. B **75**, 224421 (2007).
[37] J. X. Ma, D. Mazumdar, G. Kim, H. Sato, N. Z. Bao, and A. Gupta, J. Appl. Phys. **108**, 063917 (2010).
[38] N. M. Caffrey, T. Archer, I. Rungger, and S. Sanvito, Phys. Rev. B **83**, 125409 (2011).
[39] N. M. Caffrey, T. Archer, I. Rungger, and S. Sanvito, Phys. Rev. Lett. **109**, 226803 (2012).
[40] Y. Miura, S. Muramoto, K. Abe, and M. Shirai, Phys. Rev. B **86**, 024426 (2012).
[41] J. Zhang, X.-G. Zhang, and X. F. Han, Appl. Phys. Lett. **100**, 222401 (2012).